Chapter 5
Topology and Geometry of 3-Band Models

Ching Hua Lee and Chien Hao Tan

Abstract Berry curvature is a property of N-band models which plays an analogous role of the magnetic field. The Majorana stellar representation (MSR) is a method of decomposing N-band states into multiple 2-band states, which paves way for a more intuitive geometric understanding of N-band models. We utilise the MSR to obtain a new formula for the Berry curvature of 3-band models in terms of individual contributions from each star and cross terms involving both stars, which could be insightful for investigating Berry curvature uniformity and topological behaviour of stars. We applied the MSR method to a model with uniform Berry curvature and investigated the cancellation of the divergences among three out of four of the terms to yield an overall non-divergent Berry curvature. In summary, the MSR approach aids the discovery of materials with uniform Berry curvature and is a powerful tool in the study of fractional Chern insulators (FCI).

5.1 Introduction

The study of topology in physics emerged in the late 1980s and has been an active field of study in recent literature. Historically, the concept of topological order was required to explain the chiral spin state in high-temperature superconductivity after it was discovered that Landau's spontaneous symmetry breaking was unable to do so. And more recently, the 2016 Nobel Prize has been awarded to David J. Thouless, J. Michael Kosterlitz and F. Duncan M. Haldane for "theoretical discoveries of topological phase transitions and topological phases of matter" [1].

Researchers study topological physics for their robustness to environmental noise and impurities. For instance, topological insulators, which we study in this paper, have potential applications for quantum computing. Imagine a thin film of electrons

C. H. Lee
Department of Physics, National University of Singapore, Singapore 117542, Singapore

C. H. Tan (✉)
1 Raffles Institution Ln, Bishan 575954, Singapore
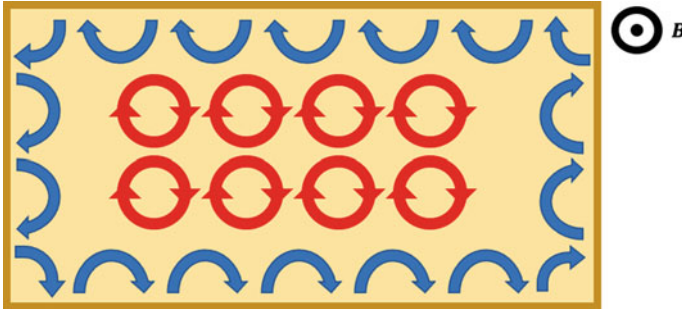e-mail: tanchienhao@gmail.com

Fig. 5.1 When a thin film of electrons is exposed to an external magnetic field, electrons in the middle will be in bound orbits, resulting in a current (red). While electrons at the edges will scatter off the edge while orbiting, resulting in an edge current (blue) that is robust to material impurities
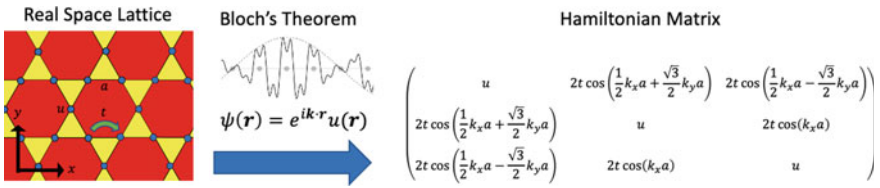

Fig. 5.2 An illustration of the Kagome lattice being converted into an 3-band model. As the lattice possesses translational symmetry, Bloch's theorem can be used to transform the real space tight-binding model into momentum space. The resultant 3-by-3 matrix is then diagonalised to obtain eigensolutions

in a strong magnetic field (refer to Fig. 5.1). The electrons in the middle (bulk) will be confined to circular orbits, but the electrons at the side will scatter off the edge and cause a current to flow around the edge of the material. The material's conductivity at the edge is not affected by small changes in the material, like impurities or imperfections and is therefore said to be protected by topology. In fact, this topologically protected edge conductivity is so robust that it is used to measure the fine structure constant.

5.1.1 Research Objectives

This paper investigates topological behaviour of 3-band models with the use of Majorana stellar representation (MSR). An N-band model is a theoretical model of condensed matter physics systems. Examples of condensed matter physics systems include graphene, superconductors, semiconductors, and generally solids with some crystalline or lattice structure. The value of N depends on the number of orbitals and sublattice sites one wishes to account for. Condensed matter systems, which often involve transition metals, typically involve many orbitals. Hence, the greater

the value of N, the higher the degree of accuracy of the model, although this comes at the cost of increased complexity. These condensed matter systems can effectively be simplified to an N by N (hermitian) matrix by transforming into momentum space using the method of Bloch waves (refer to Fig. 5.2) [2]. The properties of the system (i.e. Berry curvature) are then investigated by calculating the eigenvectors (which correspond to the quantum states) and eigenvalues (which correspond to the (eigen-)energy of the states) of the square matrix. Unfortunately, each N-band eigenstate is a complex N-dimensional vector which is difficult to visualise. The Majorana stellar representation (MSR) approach promises to solve this problem.

In this paper, the goal of the MSR approach is to understand the flatness of the Berry curvature of 3-band models. Berry curvature plays the analagous role of a magnetic field in topological materials. A more uniform Berry curvature leads to better behaviour, and therefore, models with a flat Berry curvature are sought after. For 2-band models, there is a lower-bound for the uniformity due to the fact that there is no map from $\mathbb{T}^2$ to $\mathbb{S}^2$ that has a perfectly uniform Jacobian [3]. For higher-band models, a perfectly uniform Berry curvature is permitted. However, perfectly uniform models are unphysical as they require infinite-distance-hopping terms. Hence, the trimming of hopping terms that are too far would result in a trade-off between Berry curvature uniformity and experimental feasibility. An example of a relatively uniform 3-band model has been found in [3], and the Hamiltonian can be found in Appendix 1. We seek to understand the flatness of the Berry curvature of this model with the MSR approach, in hope of discovering other uniform models.

As a small but important digression, in most literature, "flat models" refer to models with a flat eigenenergy spectrum. A flat energy spectrum also has desirable properties, but it is very different from a flat Berry curvature. To avoid confusion, this paper refers to models with flat Berry curvature as uniform models from hereon. A flat energy spectrum is mathematically easier to achieve than a flat Berry curvature, as one can always add/subtract the identity matrix to the Hamiltonian to translate the energy. On the other hand, a flat Berry curvature is much harder to achieve mathematically, and in some cases, even impossible (such as in 2-band models). Additionally, to further achieve flat energy or flat curvature models in an experimental setup is an even greater feat, as one is constrained by physical materials in addition to mathematical difficulty. In this paper, we only focus on the mathematical aspects of uniform models.

It is also worth mentioning that although the techniques developed in this paper is most applicable to the study of topological insulators, the MSR approach could be applied to other areas such as topolectrical circuits [4] and high-spin systems (Fig. 5.3).

5.1.2 Berry Phase, Berry Curvature, and Chern Number

To further elaborate on what is meant by "topological behaviour", we will discuss the concept of Berry curvature in this paragraph. The concept of Berry phase
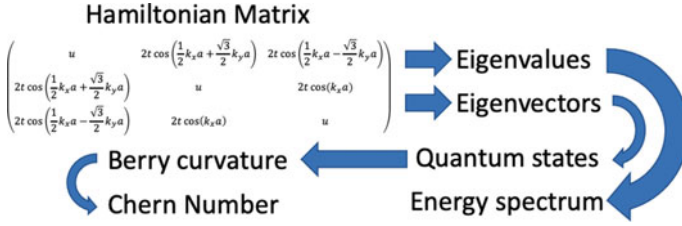
Fig. 5.3 The process of calculating the "topological behaviour" of a model

was developed in 1984 [5]. When a quantum eigenstate $|\Psi\rangle$ undergoes adiabatic cyclic evolution in parameter space (example in the proceeding paragraph), in addition to the dynamical phase $\exp(-\frac{i}{\hbar}\int_0^t dt' E(t'))$, it acquires a geometrical phase $\exp(-\oint_{\mathcal{C}} \langle\Psi| |d\Psi\rangle)$, called the Berry phase, which can be experimentally observed [5]. This also paves for the concept of a Berry connection and Berry curvature. The Berry connection is defined as $\mathcal{A} = -i \langle\Psi| |d\Psi\rangle$ and the Berry curvature $\mathcal{F} = d\mathcal{A} = -i \langle d\Psi| \wedge |d\Psi\rangle$. Application of Stokes' theorem yields an expression of Berry phase in terms of a surface integral of Berry curvature, $\gamma(\mathcal{C}) = -\oint_{\mathcal{S}} \mathcal{F}$, where $\mathcal{C} = \partial\mathcal{S}$. The Berry curvature, which can have several physical consequences [6–8], is the focus of this paper.

5.1.2.1   Spin-1/2 Particle in Magnetic Field

We provide an example of an electron in an external magnetic field to aid in explaining Berry phase, connection, and curvature. An electron is a spin-1/2 particle, and its quantum behaviour is governed by the Hamiltonian $H \propto \boldsymbol{\sigma} \cdot \mathbf{B}$ and the Schrodinger equation $H |\Psi\rangle = i\hbar\frac{\partial}{\partial t} |\Psi\rangle$. This Hamiltonian is the potential energy of the electron in a magnetic field, and the quantum state of the electron is given by the eigenvectors to the Hamiltonian. We choose to present only the positive energy eigenstate for this paper as the method is easily applied to other eigenstates. Since the Hamiltonian is dependent on the direction of the magnetic field $\mathbf{B} = (B_x, B_y, B_z) \in \mathbb{R}^3$, the eigenvectors also depend on the magnetic field. The magnetic field is the parameter space for this example. A varying magnetic field would cause the eigenstate to vary, and we ascribe an eigenstate to each corresponding point in parameter space. Calculating the eigenstate for spin-1/2 particles is achieved by decomposing the 2×2 hermitian matrix H into a combination of pauli matrices.

$$H \propto B_x\sigma_1 + B_y\sigma_2 + B_z\sigma_3 \tag{5.1}$$

$$\sigma_1 = \begin{pmatrix} 0 & 1 \\ 1 & 0 \end{pmatrix} \quad \sigma_2 = \begin{pmatrix} 0 & -i \\ i & 0 \end{pmatrix} \quad \sigma_3 = \begin{pmatrix} 1 & 0 \\ 0 & -1 \end{pmatrix} \tag{5.2}$$
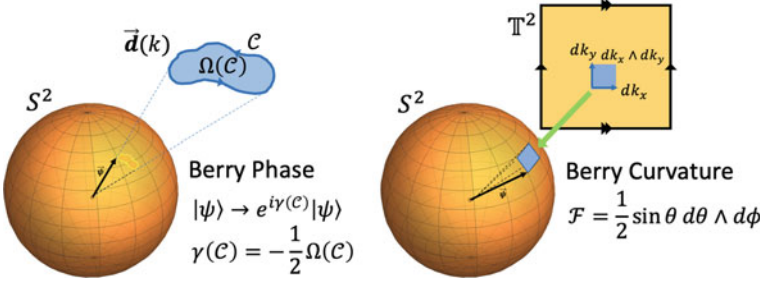
Fig. 5.4 Visualisations of the Berry phase and curvature of 2-band models. The Berry phase is acquired after a cyclic evolution in parameter space, and it can be thought of as (minus half) the solid angle of the path. The Berry curvature can be regarded as the Berry phase of a infinitesimal loop, and is hence (half) the differential solid angle (in spherical coordinates)

$$|\Psi(\mathbf{B})\rangle = \begin{pmatrix} B_z + |\mathbf{B}| \\ B_x + i B_y \end{pmatrix} \tag{5.3}$$

After an adiabatic evolution along a cyclic path $\mathcal{C}$ in parameter space, the eigenstate returns to its original value, but it picks up a phase factor $e^{i\alpha}$. This phase factor consists of two parts, the dynamical term $\exp(-\frac{i}{\hbar} \int_0^t dt' E(\mathbf{B}(t')))$ and the geometrical term $\exp(i\gamma(\mathcal{C})) = \exp(-\oint_{\mathcal{C}} \langle\Psi| |\nabla_B \Psi\rangle \cdot dB)$. The geometrical term is only a function of the cyclic path traced out by the eigenstate and does not involve the time taken for cyclic evolution.

Moreover, we consider $\mathbf{B} = B_0 \begin{pmatrix} \sin\theta \cos\phi \\ \sin\theta \sin\phi \\ \cos\theta \end{pmatrix}$ in polar coordinates, then the eigenstate can be written as $|\Psi(\mathbf{B}(\theta, \phi))\rangle = \begin{pmatrix} \cos\theta/2 \\ e^{i\phi} \sin\theta/2 \end{pmatrix}$. The eigenstate $|\Psi\rangle$ is represented on the Bloch sphere as $\mathbf{\Psi} = \begin{pmatrix} \sin\theta \cos\phi \\ \sin\theta \sin\phi \\ \cos\theta \end{pmatrix} \in S^2$. As a mathematical interlude, the Bloch sphere representation owes its existence to the fact that the space of quantum states $\mathbb{C}^2/U(1) \sim \mathbb{CP}^1 \sim S^2$ is isomorphic to the 2-sphere topologically. The Bloch sphere representation is elegant because the Berry curvature of 2-band models can be interpreted as the differential solid angle on the Bloch sphere $\mathcal{F} = \text{Im} \langle d\Psi| \wedge |d\Psi\rangle = \frac{1}{2} \sin\theta \, d\theta \wedge d\phi$. Therefore, the Berry phase of a cyclic evolution of the magnetic field is interpreted as the solid angle traced out by the cyclic path $\gamma(\mathcal{C}) = -\frac{1}{2}\Omega(\mathcal{C})$ (refer to Fig. 5.4).

5.1.2.2 *N*-Band Models

For condensed matter physics models, the parameter space is $(k_x, k_y) \in \mathbb{T}_2$ because (crystal) momentum is 2π-periodic. The Berry curvature is $\mathcal{F} = \text{Im} \langle d\Psi| \wedge |d\Psi\rangle =$
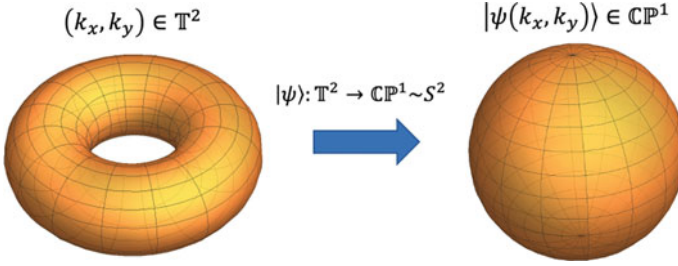
Fig. 5.5 The 2-band eigenstate is a map from the 2-torus to the 2-sphere. Maps from $\mathbb{T}^2$ to S^2 can be characterised by a winding number called the Chern number

$\mathrm{Im}(\langle \partial_x \Psi | \, | \partial_y \Psi \rangle - \langle \partial_y \Psi | \, | \partial_x \Psi \rangle) \mathrm{d}k_x \wedge \mathrm{d}k_y = F_{xy} \mathrm{d}k_x \wedge \mathrm{d}k_y$. And the Chern number of N-band models is defined as $C = 1/2\pi \int_{BZ} F_{xy} d^2 k$. N-band condensed matter physics models are analogous to spin-$((N-1)/2)$ systems as the Hamiltonians of both systems are of the same size. 2-band models, which describe physical systems like polyacetylene (Su-Schrieffer-Heeger) [9], are analogous to spin-1/2 systems. One simply replaces the magnetic field **B** with the analogous vector $\mathbf{d}(k)$. Therefore, the calculations in the previous subsection on spin-1/2 particles carry over to 2-band models. The Chern number of 2-band models is thus quantised in integer values, since the total solid angle swept out by the eigenstate on the Bloch sphere is a multiple of 4π. As we have seen, the Bloch sphere representation of 2-band (or spin-1/2) states offers insights into its Berry curvature (refer to Fig. 5.5). The generalisation of the Bloch sphere representation for higher-band models is the goal of this paper. Specifically, we work on 3-band models where eigenstates live in $\mathbb{CP}^2 \sim (S^2 \times S^2)/\mathcal{S}_2$.

5.2 The Majorana Stellar Representation for N-Band Models

The Bloch sphere representation for the 2-band state is not immediately generalisable to higher-band models. However, the Majorana stellar representation (MSR) has potential to pave a geometrical intuition for higher-band models. The MSR has already been used to understand the Berry phase of higher-spin systems [10, 11], but the application of the MSR to Berry curvature has not been studied in-depth, and is therefore the goal of this paper. The MSR allows one to decompose an N-band state into $(N-1)$ entangled 2-band states (refer to Fig. 5.6). The Berry curvature, which we will derive later, will comprise of solid angles from the individual stars, as well as correlation terms. The contribution that only involve single stars have a simple geometrical interpretation, and therefore, the MSR has hope of allowing us to explore the geometry of higher-band models in a more intuitive manner.

From [12], an N-band state $\left| \Psi^{(N)} \right\rangle = \sum_{m=1}^{N} \Psi_m |m\rangle$ can be represented as $N-1$
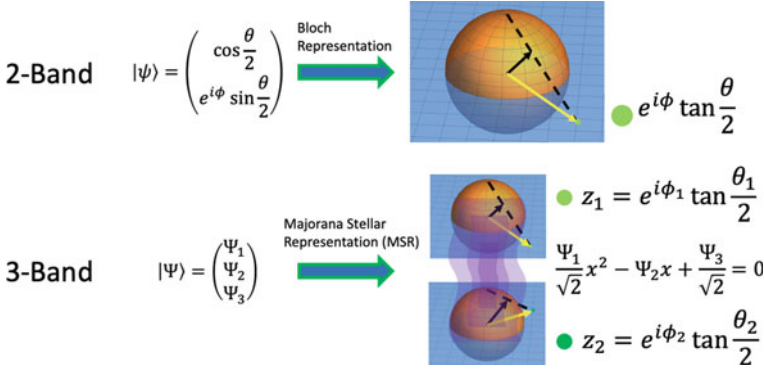
Fig. 5.6 2-band states can be projected onto the Bloch sphere. By MSR, 3-band states can be represented on 2 Bloch spheres as 2 entangled Majorana stars. The stars are given by roots to (5.4) followed by a stereographic projection from the complex plane to 2-sphere

stars on the Bloch sphere, $|u_i\rangle = \begin{pmatrix} \cos\theta_i/2 \\ e^{i\phi_i}\sin\theta_i/2 \end{pmatrix}$, with θ_i, ϕ_i given by the roots $x_i = e^{i\phi_i}\tan\frac{\theta_i}{2}$ to the polynomial $\sum_{k=1}^{N} \frac{(-1)^{k+1}\Psi_k}{\sqrt{(N-k)!(k-1)!}}x^{N-k} = 0$. Kindly refer to Appendix 2 for a more in-depth explanation.

For 3-band models, the 2 stars can be calculated by finding the roots to

$$\frac{\Psi_1}{\sqrt{2}}x^2 - \Psi_2 x + \frac{\Psi_3}{\sqrt{2}} = 0 \tag{5.4}$$

where Ψ_i are the components to the 3-component eigenstate $|\Psi\rangle$. The roots

$$x_{1,2} = \frac{\sqrt{2}\Psi_2 \pm \sqrt{2\Psi_2^2 - 4\Psi_1\Psi_3}}{2\Psi_1} \tag{5.5}$$

can be used to find the angles of the stars $|A\rangle$, $|B\rangle$ when represented on the Bloch sphere, $x_i = \tan\frac{\theta_i}{2}e^{i\phi_i}$, via stereographic projection from the complex plane to the 2-sphere (refer to Fig. 5.6). It is also important to note that due to the branch cuts of the square root function, star $|A\rangle$ and star $|B\rangle$ interchange along paths in the Brillouin zone. Kindly refer to Fig. 5.13 for a visual illustration. This exchange is later reflected in the calculation of Chern number for the individual stars.

5.3 Analysis of Uniform 3-Band Model with MSR

In this section, we investigate the uniform model obtained in [3]. The Hamiltonian can be found in Appendix 1.

An eigenstate of a 3-band model $|\Psi\rangle$ can be decomposed into 2 Majorana Stars $|A\rangle$, $|B\rangle$. The Berry curvature of 3-band models can be decomposed into 4 terms. The derivation is found in Appendix 3. The terms are grouped in the following way so as to allow for the most illuminating geometric interpretation. T_1 and T_2 have a simple geometric interpretation. T_1 and T_2 are half the differential solid angle subtended by stars A and B, respectively. However, a simple geometric interpretation for T_3 and T_4 has not been found. When we calculate the Chern number for T_1 and T_2 for the uniform model, we obtained 1.5 for both. If each star came from its own 2-band model, this Chern number would be an integer. However, the fact that it is not an integer is due to the mixing and entanglement of the 2 stars as mentioned earlier (refer to Fig. 5.13) in Sect. 5.2.

$$\text{Im}\,\langle d\Psi| \wedge |d\Psi\rangle = T_1 + T_2 + T_3 + T_4 \tag{5.6}$$
$$T_1 = \text{Im}\,\langle dA| \wedge |dA\rangle$$
$$T_2 = \text{Im}\,\langle dB| \wedge |dB\rangle$$
$$T_3 = \frac{1}{4}\frac{d(A \times B) \wedge d(A - B)}{N_2^2}$$
$$T_4 = \frac{1}{8}\frac{(A \times B) \cdot d(A - B) \wedge d(A \cdot B)}{N_2^4}$$

We proceed to plot the T_1, T_2, T_3, T_4 terms separately as shown in Figs. 5.7, 5.8, 5.9 and 5.10. Figures 5.11 and 5.12 verify the correctness of the formula.

5.3.1 Cancellation of Divergences in the Terms

The total Berry curvature is relatively flat as we are calculating the Berry curvature for the uniform model. However, the individual terms T_1, T_2, T_3 are not flat as there are divergences (points where the value goes go infinity). It is observed that there are four points of divergence for T_1, T_2, T_3 each. These four divergences are symmetric about $k_x = \pi$ and $k_y = \pi$, and the location is numerically calculated to be around $k_x = k_y = 0.4219322\pi$, where $f(k_x, k_y) := 2\Psi_2^2 - 4\Psi_1\Psi_3 = 0$. Since the total Berry curvature does not have any divergences, the first 3 terms' (T_1, T_2, T_3) divergences must cancel to result in a non-divergent Berry curvature. We investigate this cancellation in the next paragraph.

To investigate the divergences near $k_x = k_y = 0.42\pi$ (which we call k_0 from hereon for convenience) for T_1, T_2, T_3, we proceed to plot $\Psi_1(k_x, k_y)$, $\Psi_2(k_x, k_y)$, $f(k_x, k_y)$ from $k_x = k_y = 0.41\pi$ to $k_x = k_y = 0.43\pi$. From the graphs (Figs. 5.14a, 5.15 and 5.16b), we observe that Ψ_1 and Ψ_2 are relatively smooth, whereas $f(k_x, k_y)$ can be approximated as $f \propto (k_x - k_0) + i(k_y - k_0)$.
Plugging this approximation for f into T_1, T_2 and T_3 explains the existence as well as the cancellation of divergences near $k_0 = 0.42\pi$. We shall begin this process.
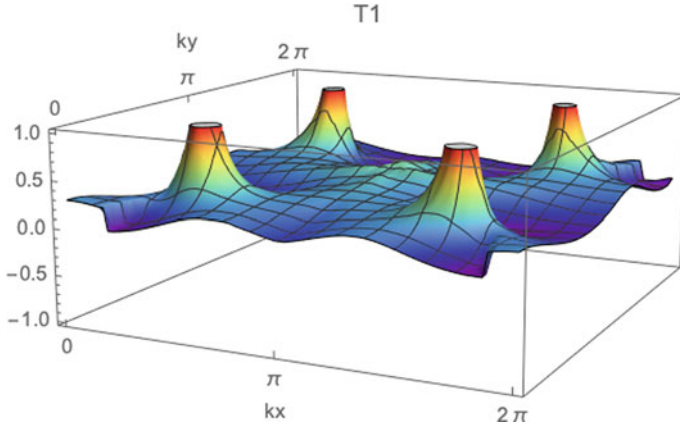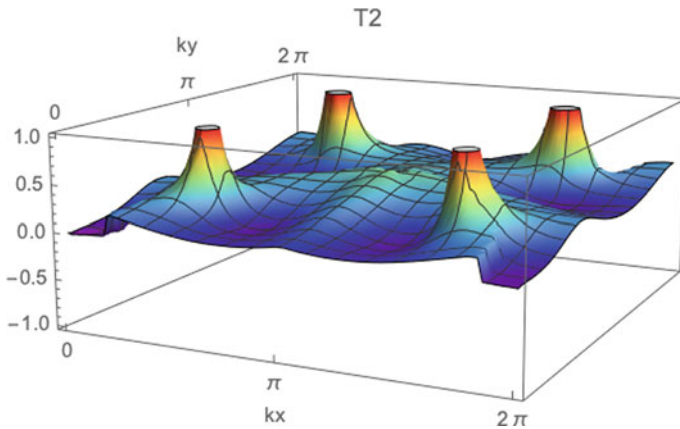
Fig. 5.7 Plot of T_1

Fig. 5.8 Plot of T_2

Firstly, by stereographic projection of the Bloch sphere onto the complex plane, we obtain T_1, T_2 in terms of $\alpha_1 = \operatorname{Re}(z_1)$, $\alpha_2 = \operatorname{Im}(z_1)$, $\beta_1 = \operatorname{Re}(z_2)$, $\beta_2 = \operatorname{Im}(z_2)$ [refer to Eqs. (5.3.1) and (5.3.1)]. Then, we look at the T_3 term, decomposing Eq. (5.9) into 6 pairwise (α_1, α_2, β_1, β_2, 4 choose 2) wedge products (refer to Eq. (5.44) in Appendix 4.

$$
\begin{aligned}
T_1 &= \operatorname{Im} \langle \mathrm{d}A| \wedge |\mathrm{d}A\rangle \\
&= \frac{2}{(1 + \alpha_1^2 + \alpha_2^2)^2} \mathrm{d}\alpha_1 \wedge \mathrm{d}\alpha_2
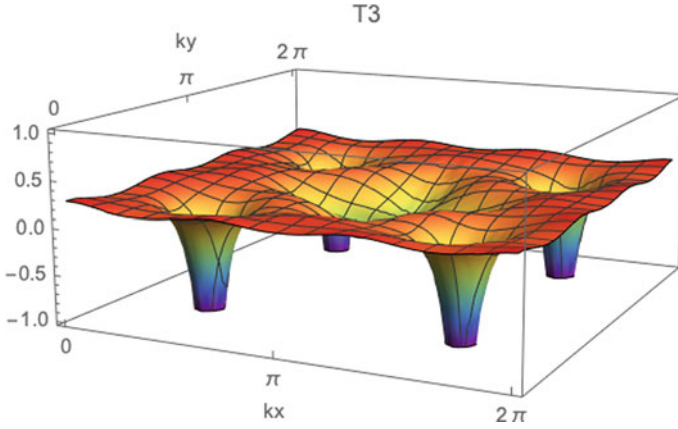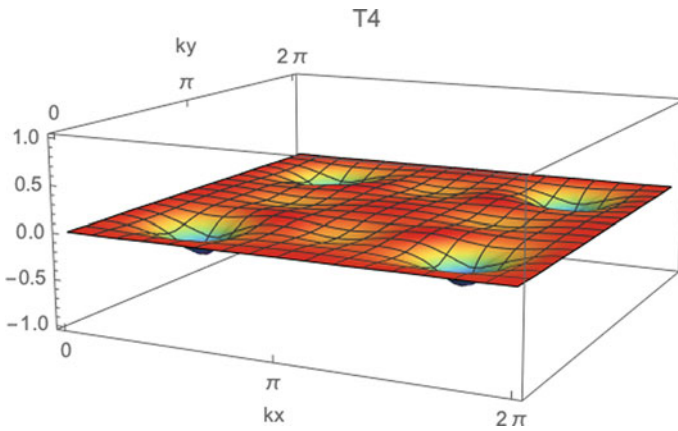\end{aligned}
\tag{5.7}
$$

Fig. 5.9 Plot of T_3

Fig. 5.10 Plot of T_4

$$T_2 = \text{Im} \langle dB| \wedge |dB \rangle$$

$$= \frac{2}{(1 + \beta_1^2 + \beta_2^2)^2} d\beta_1 \wedge d\beta_2 \tag{5.8}$$

$$T_3 = \frac{1}{4N_2^2} d(A \times B) \wedge d(A - B) \tag{5.9}$$

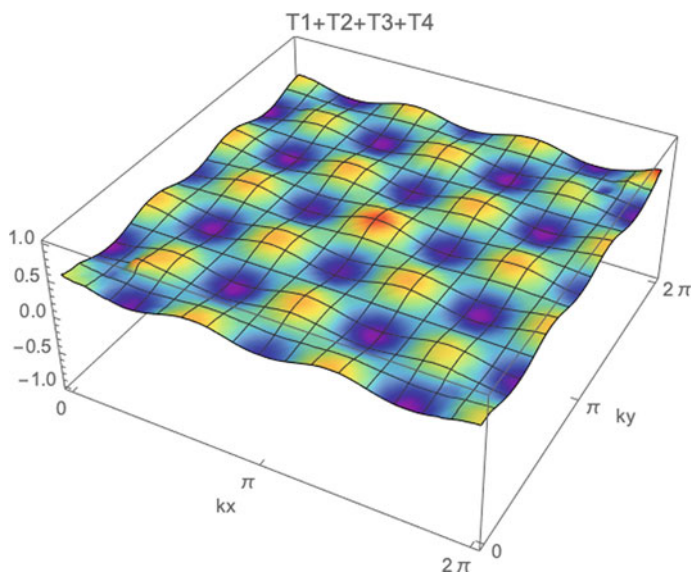$$\text{where } N_2^2 = \frac{3}{2} + \frac{1}{2} A \cdot B \tag{5.10}$$
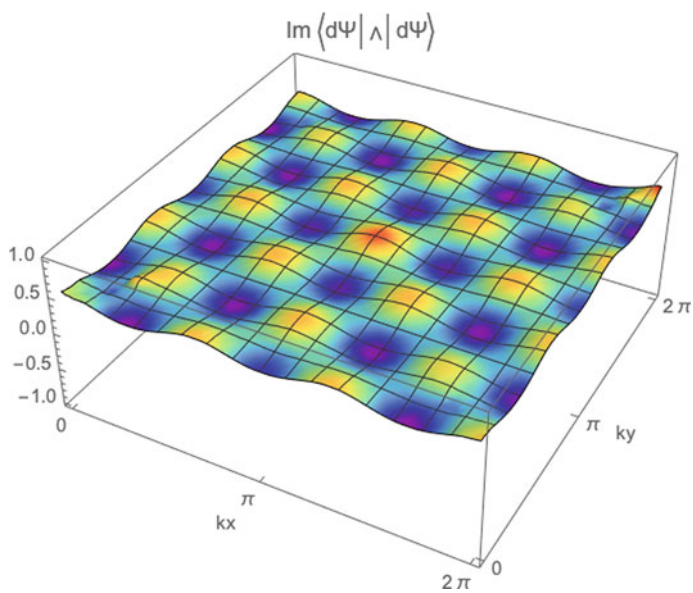
Fig. 5.11 Plot of $T_1 + T_2 + T_3 + T_4$

Fig. 5.12 Plot of $\mathrm{Im}\,\langle d\Psi | \wedge | d\Psi \rangle$

Table 5.1 Decomposition of T_1, T_2, T_3 into wedge products. $\Gamma := 1 + \alpha_1^2 + \alpha_2^2$

Term/ coefficient of	$d\alpha_1 \wedge d\alpha_2$	$d\alpha_1 \wedge d\beta_1$	$d\alpha_1 \wedge d\beta_2$	$d\alpha_2 \wedge d\beta_1$	$d\alpha_2 \wedge d\beta_2$	$d\beta_1 \wedge d\beta_2$
T_1	$\frac{2}{\Gamma^2}$	0	0	0	0	0
T_2	0	0	0	0	0	$\frac{2}{\Gamma^2}$
T_3	$-\frac{1}{\Gamma^2}$	0	$\frac{1}{\Gamma^2}$	$-\frac{1}{\Gamma^2}$	0	$-\frac{1}{\Gamma^2}$

Evaluating the partial derivatives found in Eq. (5.44) is a straightforward but tedious process, which can be achieved with the help of symbolic Mathematica. Moreover, because we are focussed on $k_0 = 0.42\pi$ where $f = 0$ and therefore $z_1 = z_2$ ($\alpha_1 = \beta_1$, $\alpha_2 = \beta_2$), the massive expressions turn out to simplify greatly. We present the simplification of $\partial_{\alpha_1}(A \times B)\partial_{\alpha_2}(A - B) - \partial_{\alpha_2}(A \times B)\partial_{\alpha_1}(A - B)$ in detail [refer to Eqs. (5.45)–(5.52)] of Appendix 5 but provide only the result for the other 5 terms (refer to Table 5.1). We look at the divergent terms of $d\alpha_1 \wedge d\alpha_2$, $d\alpha_1 \wedge d\beta_2$, $d\alpha_2 \wedge d\beta_2$, $d\beta_1 \wedge d\beta_2$ (because they have non-zero coefficient in T_1, T_2, T_3). In order to evaluate the wedge products like $d\alpha_1 \wedge d\alpha_2$, we make use of the approximation for f near k_0.

$$f(k_x, k_y) \approx 1.85 e^{-i0.7\pi}((k_x - k_0) + i(k_y - k_0)) \tag{5.11}$$

Evaluating partial derivatives and neglecting non-divergent terms (Appendix 6), we observe there are two types of terms responsible for divergence at k_0: (a) The $1/\sqrt{(k_x - k_0)^2 + (k_y - k_0)^2}$ term and (b) the $1/\sqrt{(k_x - k_0) - i(k_y - k_0)}$ term. Both need to have coefficients (from T_1, T_2, T_3) that cancel in order for the Berry curvature to be non-divergent.

$$D_1 := \frac{1.85}{16\Psi_1^2} \frac{1}{\sqrt{(k_x - k_0)^2 + (k_y - k_0)^2}} \tag{5.12}$$

$$D_2 := \text{Re}\left[\frac{\sqrt{1.85 e^{+i0.7\pi}}}{\sqrt{2}\Psi_1} \partial_z\left(\frac{\Psi_2}{\Psi_1}\right)\frac{1}{\sqrt{(k_x - k_0) - i(k_y - k_0)}}\right] \tag{5.13}$$

$$D_3 := \text{Re}\left[\frac{\sqrt{1.85 e^{+i0.7\pi}}}{\sqrt{2}\Psi_1} \partial_z\left(\frac{\bar{\Psi}_2}{\Psi_1}\right)\frac{1}{\sqrt{(k_x - k_0) - i(k_y - k_0)}}\right] \tag{5.14}$$

From Table 5.2, the cancellation of divergent terms is observed. This concludes our discussion.

Table 5.2 Coefficients of divergent terms D_1, D_2, D_3 in T_1, T_2, T_3. We observe that all coefficients cancel when T_1, T_2, T_3 is added up. $\Gamma := 1 + \alpha_1^2 + \alpha_2^2$

		D_1	D_2	D_3
T_1	$d\alpha_1 \wedge d\alpha_2$	$\frac{2}{\Gamma^2}$	$\frac{2}{\Gamma^2}$	
T_2	$d\beta_1 \wedge d\beta_2$	$\frac{2}{\Gamma^2}$	$-\frac{2}{\Gamma^2}$	
T_3	$d\alpha_1 \wedge d\alpha_2$	$-\frac{1}{\Gamma^2}$	$-\frac{1}{\Gamma^2}$	
	$d\alpha_1 \wedge d\beta_2$	$-\frac{1}{\Gamma^2}$		$-\frac{1}{\Gamma^2}$
	$d\alpha_2 \wedge d\beta_1$	$-\frac{1}{\Gamma^2}$		$\frac{1}{\Gamma^2}$
	$d\beta_1 \wedge d\beta_2$	$-\frac{1}{\Gamma^2}$	$\frac{1}{\Gamma^2}$	
$T_1 + T_2 + T_3$		0	0	0

5.4 Conclusion

In this paper, we discussed concept of Berry curvature and explored a model with relatively uniform Berry curvature from [3] using the Majorana stellar representation (MSR). We observed and explained analytically the cancellations of divergences in the Berry curvatures T_1–T_3. Overall, the key result of this paper is the development of the MSR method (Eq. 5.6) and the cancellation of divergences when the MSR method is applied to the uniform model in [3].

5.5 Further Work

As the MSR method for Berry curvature has not been explored extensively, there is still plenty of room for further research. We are currently generalising the divergences analysis to any model and investigating the switching of the stars. The discriminant function $f(k_x, k_y)$ is also promising, and exceptional points (points where $f = 0$) hint at the possibility of Riemann surfaces and topological characterisation.

Appendix 1: Hamiltonian of Uniform 3-Band Model

$$
H = \begin{pmatrix}
\frac{51}{76} + \frac{2\cos k_x}{15} + \frac{2\cos k_y}{15} - \frac{2\cos k_x \cos k_y}{45} \\
-\frac{3\sin k_x}{38} + \frac{4\cos k_y \sin k_x}{31} + \left(-\frac{3\sin k_y}{38} + \frac{4\cos k_x \sin k_y}{31}\right) i \\
-\frac{3\cos k_x}{25} + \frac{3\cos k_y}{25} - \frac{\sin k_x \sin k_y}{7} i \\[2mm]
-\frac{3\sin k_x}{38} + \frac{4\cos k_y \sin k_x}{31} + \left(\frac{3\sin k_y}{38} - \frac{4\cos k_x \sin k_y}{31}\right) i \\
\frac{63}{95} - \frac{4\cos k_x}{41} - \frac{4\cos k_y}{41} - \frac{2\cos k_x \cos k_y}{17} \\
-\frac{5\sin k_x}{33} - \frac{\cos k_y \sin k_x}{15} + \left(-\frac{5\sin k_y}{33} - \frac{\cos k_x \sin k_y}{15}\right) i \\[2mm]
-\frac{3\cos k_x}{25} + \frac{3\cos k_y}{25} + \frac{\sin k_x \sin k_y}{7} i \\
-\frac{5\sin k_x}{33} - \frac{\cos k_y \sin k_x}{15} + \left(\frac{5\sin k_y}{33} + \frac{\cos k_x \sin k_y}{15}\right) i \\
\frac{2}{3} - \frac{\cos k_x}{28} - \frac{\cos k_y}{28} + \frac{4\cos k_x \cos k_y}{25}
\end{pmatrix}
$$

Appendix 2: Derivation of the Majorana Stellar Representation (MSR)

2.1 Schwinger Boson Representation

We begin by first discussing the Schwinger Boson Representation for spin-J quantum systems [13]. A spin-J Hilbert space is characterised by a basis and spin operators that act on the basis states. Namely, the $(2J + 1)$-dimensional space has basis states given by $|J, m\rangle$, $m \in \{-J, -J + 1, ..., J - 1, J\}$. Spin operators S^+, S^-, S^2, S_z act on these basis states in the following way.

$$S^+ |J, m\rangle = \sqrt{J(J + 1) - m(m + 1)} \, |J, m + 1\rangle \tag{5.15}$$

$$S^- |J, m\rangle = \sqrt{J(J + 1) - m(m - 1)} \, |J, m - 1\rangle \tag{5.16}$$

$$S^2 |J, m\rangle = J(J + 1) |J, m\rangle \tag{5.17}$$

$$S_z |J, m\rangle = m |J, m\rangle \tag{5.18}$$

The spin operators also obey the $\mathfrak{su}(2)$ Lie algebra.

$$S_x := \frac{1}{2}(S^+ + S^-) \tag{5.19}$$

$$S_y := \frac{1}{2i}(S^+ - S^-) \tag{5.20}$$

$$[S_i, S_j] = i\epsilon_{ijk} S_k \tag{5.21}$$

It turns out, we can define two bosonic modes and use a clever definition of the spin operators to achieve the same commutation relations and basis states. If we define $[a, a^\dagger] = [b, b^\dagger] = 1$ (all other commutation relations vanish), and

$$S^+ = a^\dagger b \tag{5.22}$$

$$S^- = b^\dagger a \tag{5.23}$$

$$S_z = \frac{1}{2}(a^\dagger a - b^\dagger b) \tag{5.24}$$

then we can obtain the commutation relations

$$[S^+, S^-] = 2S_z \tag{5.25}$$

$$[S_z, S^+] = +S^+ \tag{5.26}$$

$$[S_z, S^-] = -S^- \tag{5.27}$$

which is exactly Eq. (5.21) after some manipulation.

Additionally, if we define the basis states as

$$|J, m\rangle = \frac{(a^\dagger)^{J+m}}{\sqrt{(J+m)!}} \frac{(b^\dagger)^{J-m}}{\sqrt{(J-m)!}} |\Omega\rangle \tag{5.28}$$

then one can check that it satisfies the following Eqs. (5.15)–(5.18) even with the new definitions (5.22)–(5.24). Equation (5.28) is the Schwinger Boson Representation for spin-J states in terms of 2 bosonic modes.

2.2. Majorana Stellar Representation

The Majorana Stellar Representation is simply a factorisation after converting a spin-J system to its Schwinger Boson Representation [12]. Let a spin-J quantum state be written in terms of the basis states $|J, m\rangle$ using Schwinger bosons.

$$|\Psi\rangle = \sum_{m=-J}^{J} C_m |J, m\rangle \tag{5.29}$$

$$= \sum_{m=-J}^{J} \frac{C_m (a^\dagger)^{J+m} (b^\dagger)^{J-m}}{\sqrt{(J+m)!(J-m)!}} |\Omega\rangle \tag{5.30}$$

We may factorise (5.30) in the following way (5.31). The $2J$ complex numbers z_i completely characterise the spin-J state. Moreover, when we stereographically project the complex numbers z_i onto the 2-sphere, we obtain $2J$ points in the Bloch sphere, which we call the Majorana Stars.

$$|\Psi\rangle = \frac{C_J}{\sqrt{(2J)!}} \prod_{i=1}^{2J} (a^\dagger + z_i b^\dagger) |\Omega\rangle \tag{5.31}$$

$$= \frac{C_J}{\sqrt{(2J)!}} \left[(a^\dagger)^{2J} + (a^\dagger)^{2J-1} b^\dagger \left(\sum_{i=1}^{2J} z_i \right) \right.$$
$$\left. + (a^\dagger)^{2J-2} (b^\dagger)^2 \left(\sum_{i<j} z_i z_j \right) + \dots + (b^\dagger)^{2J} \left(\prod_i z_i \right) \right] \tag{5.32}$$

Comparing coefficients of Eqs. (5.30) and (5.32).

$$m = J - 1: \frac{C_{J-1}}{\sqrt{(2J-1)!}} = \frac{C_J}{\sqrt{(2J)!}} \sum_i z_i \tag{5.33}$$

$$m = J - 2: \frac{C_{J-2}}{\sqrt{(2J-2)!2!}} = \frac{C_J}{\sqrt{(2J)!}} \sum_{i<j} z_i z_j \tag{5.34}$$

$$m = J - 3: \frac{C_{J-3}}{\sqrt{(2J-3)!3!}} = \frac{C_J}{\sqrt{(2J)!}} \sum_{i<j<k} z_i z_j z_k \tag{5.35}$$

$$\dots \tag{5.36}$$

$$m = -J: \frac{C_{-J}}{\sqrt{(2J)!}} = \frac{C_J}{\sqrt{(2J)!}} \prod_i z_i \tag{5.37}$$

Now, in order to find the values of z_i, $1 \le i \le 2J$ that satisfy Eqs. (5.33)–(5.37), we consider the polynomial equation with z_i as roots,

$$0 = \prod_{i=1}^{2J} (x - z_i) \tag{5.38}$$

$$= x^{2J} - x^{2J-1} \left(\sum_i z_i \right) + x^{2J-2} \left(\sum_{i<j} z_i z_j \right)$$
$$- x^{2J-3} \left(\sum_{i<j<k} z_i z_j z_k \right) + \dots + (-1)^{2J} \left(\prod_i z_i \right) \tag{5.39}$$

and substituting (5.33) to (5.37) into (5.39) yields

$$\sum_{k=0}^{2J} \frac{(-1)^k C_{J-k} x^{2J-k}}{\sqrt{(2J-k)!k!}} = 0 \tag{5.40}$$

Appendix 3: Derivation of Berry Curvature in Terms of Majorana Stars ($N = 3$)

We denote the stars for $N = 3$ models by $|A\rangle$ and $|B\rangle$. Starting from the expression from [10].

$$\text{Im}\,\langle\Psi|\,|d\Psi\rangle = \text{Im}\,\langle A|\,|dA\rangle + \text{Im}\,\langle B|\,|dB\rangle + \frac{1}{4}\frac{(A \times B) \cdot d(A - B)}{N_2^2}$$

where $N_2^2 = 1 + \langle A|\,|B\rangle\,\langle B|\,|A\rangle = \frac{3}{2} + \frac{1}{2}(A \cdot B)$. To find $\mathcal{F} = \text{Im}\,\langle d\Psi|\wedge|d\Psi\rangle$, we take the exterior derivative of the Berry phase.

$$\mathcal{F} = \text{Im}\,\langle d\Psi|\wedge|d\Psi\rangle \tag{5.41}$$

$$\mathcal{F} = \text{Im}\,d\,\langle\Psi|\,|d\Psi\rangle \tag{5.42}$$

$$\mathcal{F} = \text{Im}\,\langle dA|\wedge|dA\rangle + \text{Im}\,\langle dB|\wedge|dB\rangle \tag{5.43}$$

$$+ \frac{1}{4}\frac{d(A \times B) \wedge d(A - B)}{N_2^2}$$

$$+ \frac{1}{8}\frac{(A \times B) \cdot d(A - B) \wedge d(A \cdot B)}{N_2^4}$$

Appendix 4: Decomposition of T_3 into Wedge Products

$$T_3 = \frac{1}{4N_2^2}d(A \times B) \wedge d(A - B) \tag{5.44}$$

$$= \frac{1}{4N_2^2}[\partial_{\alpha_1}(A \times B)\partial_{\alpha_2}(A - B) - \partial_{\alpha_2}(A \times B)\partial_{\alpha_1}(A - B)]d\alpha_1 \wedge d\alpha_2$$

$$+ \frac{1}{4N_2^2}[\partial_{\alpha_1}(A \times B)\partial_{\beta_1}(A - B) - \partial_{\beta_1}(A \times B)\partial_{\alpha_1}(A - B)]d\alpha_1 \wedge d\beta_1$$

$$+ \frac{1}{4N_2^2}[\partial_{\alpha_1}(A \times B)\partial_{\beta_2}(A - B) - \partial_{\beta_2}(A \times B)\partial_{\alpha_1}(A - B)]d\alpha_1 \wedge d\beta_2$$

$$+ \frac{1}{4N_2^2}[\partial_{\alpha_2}(A \times B)\partial_{\beta_1}(A - B) - \partial_{\beta_1}(A \times B)\partial_{\alpha_2}(A - B)]d\alpha_2 \wedge d\beta_1$$

$$+ \frac{1}{4N_2^2}[\partial_{\alpha_2}(A \times B)\partial_{\beta_2}(A - B) - \partial_{\beta_2}(A \times B)\partial_{\alpha_2}(A - B)]d\alpha_2 \wedge d\beta_2$$

$$+ \frac{1}{4N_2^2}[\partial_{\beta_1}(A \times B)\partial_{\beta_2}(A - B) - \partial_{\beta_2}(A \times B)\partial_{\beta_1}(A - B)]d\beta_1 \wedge d\beta_2$$

Appendix 5: Simplification of Coefficient of $d\alpha_1 \wedge d\alpha_2$ at (k_0, k_0)

$$\partial_{\alpha_1}(A \times B)\partial_{\alpha_2}(A - B) - \partial_{\alpha_2}(A \times B)\partial_{\alpha_1}(A - B)$$

$$= -\frac{8(1 + 4\alpha_1\beta_1 - \beta_1^2 + 4\alpha_2\beta_2 - \beta_2^2 + \alpha_1^2(-1 + \beta_1^2 + \beta_2^2) + \alpha_2^2(-1 + \beta_1^2 + \beta_2^2))}{((1 + \alpha_1^2 + \alpha_2^2)^3(1 + \beta_1^2 + \beta_2^2))} \quad (5.45)$$

$$\text{At } k_x = k_y = k_0, \quad (5.46)$$

$$f(k_0, k_0) = 0 \rightarrow \quad z_1 = z_2(\alpha_1 = \beta_1, \alpha_2 = \beta_2), \quad (5.47)$$

$$f = 0 \rightarrow A = B \rightarrow A \cdot B = 1 \rightarrow \quad N_2^2(k_0, k_0) = 3/2 + 1/2 = 2 \quad (5.48)$$

$$\text{Substituting (47) into (45), it simplifies to} \quad (5.49)$$

$$\partial_{\alpha_1}(A \times B)\partial_{\alpha_2}(A - B) - \partial_{\alpha_2}(A \times B)\partial_{\alpha_1}(A - B) = -\frac{8}{(1 + \alpha_1^2 + \alpha_2^2)^2} \quad (5.50)$$

$$\text{Coefficient of } d\alpha_1 \wedge d\alpha_2 = \frac{1}{4N_2^2}$$

$$[\partial_{\alpha_1}(A \times B)\partial_{\alpha_2}(A - B) - \partial_{\alpha_2}(A \times B)\partial_{\alpha_1}(A - B)] \quad (5.51)$$

$$= -\frac{1}{(1 + \alpha_1^2 + \alpha_2^2)^2} \quad (5.52)$$

Appendix 6: Evaluation of Wedge Products

The 2 stars are given by complex roots (Eqs. 5.53 and 5.54). With the approximation of f near k_0 (Eq. 5.11), we can obtain partial derivatives $\partial_x = \frac{\partial}{\partial k_x}, \partial_y = \frac{\partial}{\partial k_y}$ of $z_1, z_2, \bar{z}_1, \bar{z}_2$. Then, by Eqs. (5.55)–(5.58), we obtain partial derivatives ∂_x, ∂_y of $\alpha_1 = \text{Re}(z_1), \alpha_2 = \text{Im}(z_1), \beta_1 = \text{Re}(z_2), \beta_2 = \text{Im}(z_2)$.

$$z_1 = \frac{\sqrt{2}\Psi_2 + \sqrt{f}}{2\Psi_1} \tag{5.53}$$

$$z_2 = \frac{\sqrt{2}\Psi_2 - \sqrt{f}}{2\Psi_1} \tag{5.54}$$

$$\alpha_1 = \frac{1}{2}(z_1 + \bar{z}_1) \tag{5.55}$$

$$\alpha_2 = \frac{1}{2i}(z_1 - \bar{z}_1) \tag{5.56}$$

$$\beta_1 = \frac{1}{2}(z_2 + \bar{z}_2) \tag{5.57}$$

$$\beta_2 = \frac{1}{2i}(z_2 - \bar{z}_2) \tag{5.58}$$

Defining $\partial_z = \frac{1}{2}(\partial_x - i\,\partial_y)$ and $\partial_{\bar{z}} = \frac{1}{2}(\partial_x + i\,\partial_y)$, listed below are the wedge products which have non-zero coefficient (refer to Table 5.1) in T_1, T_2, T_3.

$$\partial_x\alpha_1\partial_y\alpha_2 - \partial_y\alpha_1\partial_x\alpha_2 \approx \frac{1.85}{16\Psi_1^2}\frac{1}{\sqrt{(k_x - k_0)^2 + (k_y - k_0)^2}}$$
$$+ \mathrm{Re}\left[\frac{\sqrt{1.85}e^{+i0.7\pi}}{\sqrt{2}\Psi_1}\partial_z\left(\frac{\Psi_2}{\Psi_1}\right)\frac{1}{\sqrt{(k_x - k_0) - i(k_y - k_0)}}\right] \tag{5.59}$$
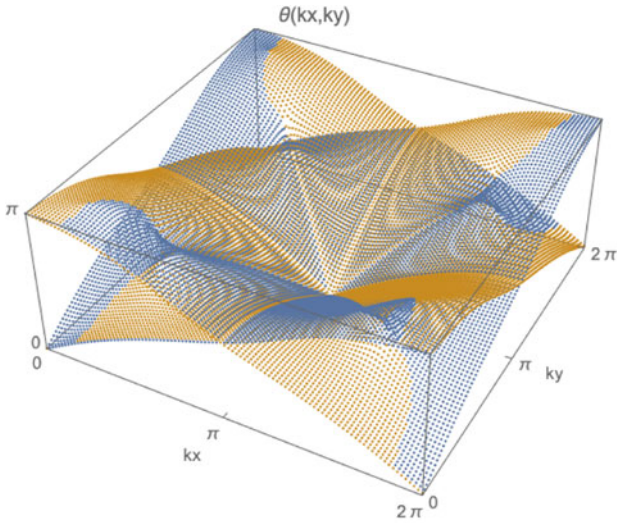
$$\partial_x\alpha_1\partial_y\beta_2 - \partial_y\alpha_1\partial_x\beta_2 \approx -\frac{1.85}{16\Psi_1^2}\frac{1}{\sqrt{(k_x - k_0)^2 + (k_y - k_0)^2}}$$
$$- \mathrm{Re}\left[\frac{\sqrt{1.85}e^{+i0.7\pi}}{\sqrt{2}\Psi_1}\partial_z\left(\frac{\bar{\Psi}}{2\Psi_1}\right)\frac{1}{\sqrt{(k_x - k_0) - i(k_y - k_0)}}\right] \tag{5.60}$$

$$\partial_x\alpha_2\partial_y\beta_1 - \partial_y\alpha_2\partial_x\beta_1 \approx \frac{1.85}{16\Psi_1^2}\frac{1}{\sqrt{(k_x - k_0)^2 + (k_y - k_0)^2}}$$
$$- \mathrm{Re}\left[\frac{\sqrt{1.85}e^{+i0.7\pi}}{\sqrt{2}\Psi_1}\partial_z\left(\frac{\bar{\Psi}_2}{\Psi_1}\right)\frac{1}{\sqrt{(k_x - k_0) - i(k_y - k_0)}}\right] \tag{5.61}$$
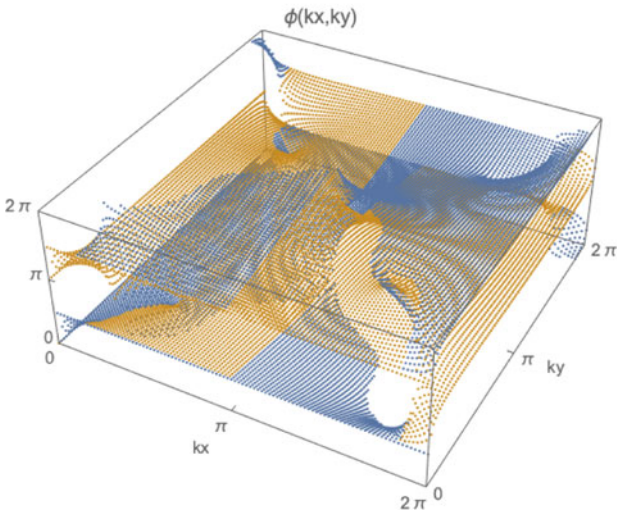
$$\partial_x\beta_1\partial_y\beta_2 - \partial_y\beta_1\partial_x\beta_2 \approx \frac{1.85}{16\Psi_1^2}\frac{1}{\sqrt{(k_x - k_0)^2 + (k_y - k_0)^2}}$$
$$- \mathrm{Re}\left[\frac{\sqrt{1.85}e^{+i0.7\pi}}{\sqrt{2}\Psi_1}\partial_z\left(\frac{\Psi_2}{\Psi_1}\right)\frac{1}{\sqrt{(k_x - k_0) - i(k_y - k_0)}}\right] \tag{5.62}$$

Appendix 7: Additional Figures

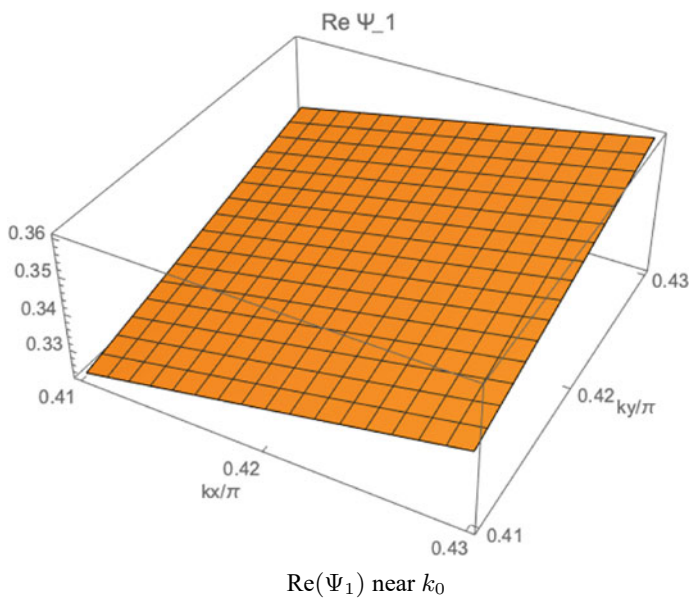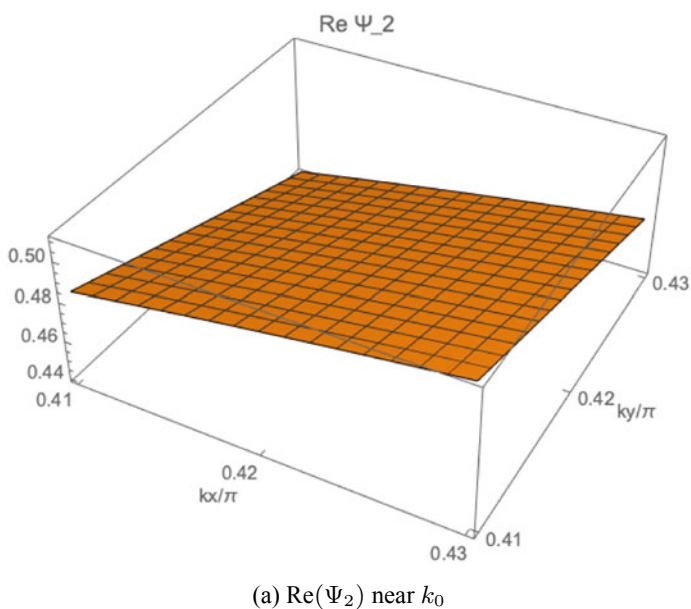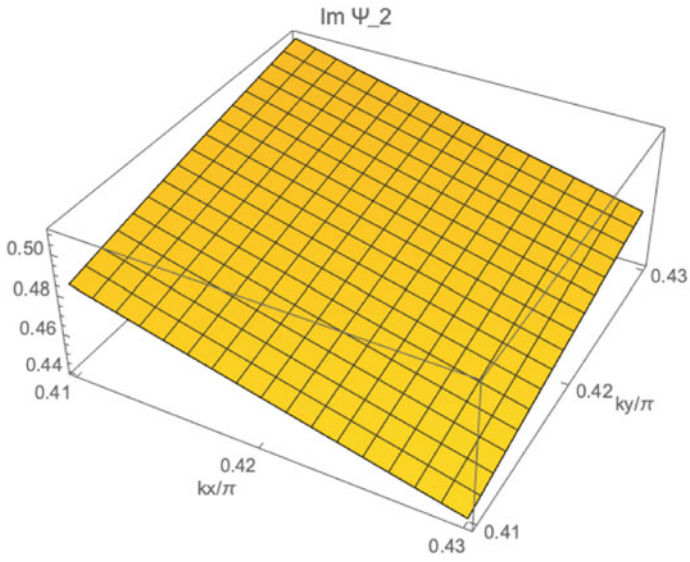See Figs. 5.13, 5.14, 5.15, and 5.16.

(a) Plot of $\theta(k_x, k_y)$
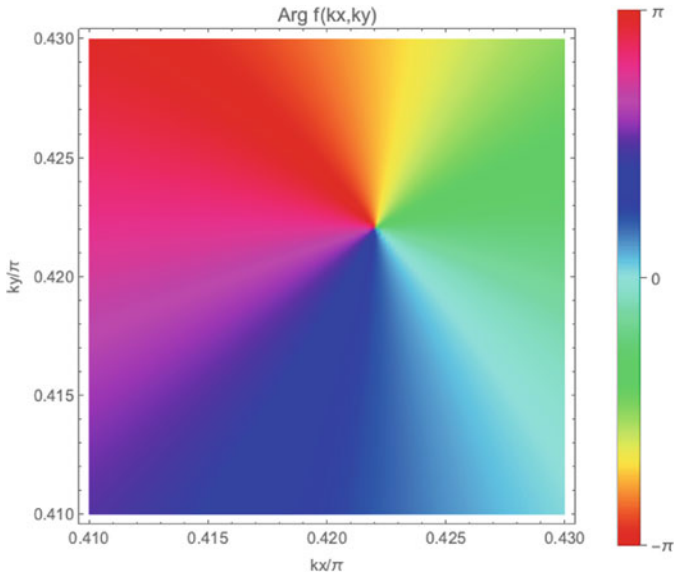

(b) Plot of $\phi(k_x, k_y)$

Fig. 5.13 Plot of θ and ϕ for both stars. The stars interchange positions as one traverses in the parameter space $\mathbb{T}^2$, and thus are said to be entangled

Re(Ψ₁) near k₀

Fig. 5.14 Plot of Ψ_1 near k_0

(a) Re(Ψ₂) near k₀

Fig. 5.15 Plot of Ψ_2 near k_0

(b) Im(Ψ_2) near k_0

Fig. 5.15 (continued)

(a) Arg(f) near k_0
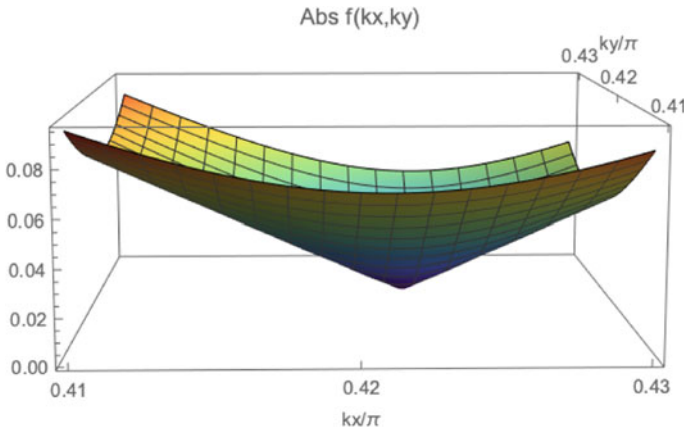
Fig. 5.16 Plot of f near k_0

(b) Abs(f) near k_0

Fig. 5.16 (continued)

References

1. Topological Phase Transitions and Topological Phases of Matter (n.d.). Retrieved January 10, 2021, from https://www.nobelprize.org/uploads/2018/06/advanced-physicsprize2016-1.pdf
2. Kittel, C. (1996). *Introduction to solid state physics*. New York: John Wiley & Sons.
3. Lee, C. H., Claassen, M., & Thomale, R. (2017). Band structure engineering of ideal fractional Chern insulators. *Physical Review B, 96*(16). https://doi.org/10.1103/physrevb.96.165150
4. Lee, C. H., Imhof, S., Berger, C., Bayer, F., Brehm, J., Molenkamp, L. W., & Thomale, R. (2018). Topolectrical Circuits. *Communications Physics, 1*(1). https://doi.org/10.1038/s42005-018-0035-2
5. Changes, Quantal Phase, & Adiabatic, Factors Accompanying. (1984). Proceedings of the Royal Society of London. *A. Mathematical and Physical Sciences, 392*(1802), 45–57. https://doi.org/10.1098/rspa.1984.0023
6. Wimmer, M., Price, H. M., Carusotto, I., & Peschel, U. (2017). Experimental measurement of the Berry curvature from anomalous transport. *Nature Physics, 13*(6), 545–550. https://doi.org/10.1038/nphys4050
7. Virk, K. S., & Sipe, J. E. (2012). Anomalous THz emission from quantum wells with optically injected Berry curvature. In *Conference on lasers and electro-optics*. https://doi.org/10.1364/qels.2012.qtu1h.7
8. Haldane, F. D. (2004). Berry curvature on the fermi surface: Anomalous hall effect as a topological fermi-liquid property. *Physical Review Letters, 93*(20). https://doi.org/10.1103/physrevlett.93.206602
9. Asboth, J. K., Oroszlany, L., & Palyi, A. (2016). A short course on topological insulators. *Lecture Notes in Physics*. https://doi.org/10.1007/978-3-319-25607-8
10. Liu, H., & Fu, L. (2014). Representation of berry phase by the trajectories of Majorana stars. *Physical Review Letters, 113*(24). https://doi.org/10.1103/physrevlett.113.240403
11. Bruno, P. (2012). Quantum geometric phase in Majorana's stellar representation: Mapping onto a many-body Aharonov-Bohm phase. *Physical Review Letters, 108*(24). https://doi.org/10.1103/physrevlett.108.240402
12. Majorana, E. (1932). Atomi orientati in campo magnetico variabile. *Il Nuovo Cimento, 9*(2), 43–50. https://doi.org/10.1007/bf02960953
13. Schwinger, J. (1965). On angular momentum. In L. Biedenharn & H. Van Dam (Eds.), *Quantum theory of angular momentum* (p. 229). New York: Academic Press.